Systematic Design of a Transimpedance Amplifier With Specified Electromagnetic Out-of-Band Interference Behavior

Marcel J. van der Horst, André C. Linnenbank, *Member, IEEE*, Wouter A. Serdijn, *Senior Member, IEEE*, and John R. Long, *Member, IEEE*

***Abstract*—In negative-feedback amplifier design, electromagnetic interference (EMI) behavior is usually completely disregarded. EMI can, e.g., result in detection of low-frequency envelope variations of the usually high-frequency interfering signals. If the detected signals end up in the pass band of the negative-feedback amplifier, they cannot be distinguished from the intended signal any longer, so the signal-to-error ratio (SER) is reduced. Several measures can be taken to prevent unacceptable reduction of the SER, like applying filters, chokes, etc. In this paper, however, circuit design aspects are investigated. It is assumed that interference reaches the amplifier input and that the SER has to be assured by a proper design of the negative-feedback amplifier. Since EMI is related to nonlinear distortion, it is a function of the loop gain of the negative-feedback amplifier. For a given electromagnetic (EM) environment it is therefore possible to calculate the minimum loop gain required to reduce EMI to acceptable levels without filtering. To illustrate this systematic design method a transimpedance amplifier is designed and built to properly function in interfering field strengths up to 30 V/m. Experimental results are in good agreement with theory.**

***Index Terms*—Envelope detection, electromagnetic interference** (EMI)**, negative-feedback amplifier, nonlinear distortion, signal-to-error ratio (SER), susceptibility, transimpedance amplifier.**

I. Introduction

DESIGNING a negative-feedback amplifier usually starts with determining the specifications of the amplifier to be designed. Electromagnetic compatibility (EMC) is a requirement that is often disregarded in the design process. Yet, with the current congestion of the electromagnetic (EM) spectrum due to electronic systems that intentionally, or unintentionally, pollute the EM environment, the interference burden for negative-feedback amplifiers increases. In order not to degrade the amplifier performance due to electromagnetic interference (EMI), EMC should be considered and incorporated in the design process.

Manuscript received July 08, 2008; revised November 06, 2008, March 12, 2009. First published June 10, 2009; current version published March 05, 2010. This paper was recommended by Associate Editor A. J. Lopez Martin.

M. J. van der Horst is with the Department of Electrical Engineering, Hogeschool van Amsterdam, Amsterdam 1000 BA, The Netherlands (e-mail: m.j.van.der.horst@hva.nl).

A. C. Linnenbank is with the Heart Failure Research Center, Academic Medical Center, University of Amsterdam, Amsterdam 1105 AZ, The Netherlands (e-mail: a.c.linnenbank@amc.uva.nl).

W. A. Serdijn and J. R. Long are with the Electronics Research Laboratory/DIMES, Delft University of Technology, Delft 2628 CD, The Netherlands (e-mail: w.a.serdijn@tudelft.nl; resp.j.r.long@tudelft.nl).

Digital Object Identifier 10.1109/TCSI.2009.2025003

In practical situations, the negative-feedback amplifier itself seldomly is a severe source of interference, but its susceptibility may be large. Therefore, this paper concentrates on reducing the amplifier susceptibility to an acceptable level. Here, EMI induced errors, by out-of-band interference, comparable to the total white noise generated by the amplifier are considered to be acceptable.

Usually, EMI is prevented by screening of wires, using chokes and applying filters reducing the disturbing out-of-band signal at the input of the amplifier. Here, as an additional, alternative, measure, it is investigated how the negative-feedback amplifier itself can be designed to have a low EMI susceptibility to the unfiltered out-of-band disturbing signal at its input, by using circuit design strategies only.

The effects of EMI on active devices like bipolar junction transistors (BJT) or FETs are closely related to second-order harmonic distortion, i.e., it is determined by the second-order nonlinearity of the device [1]. Disturbance results in dc-shifts of the bias currents and detection of the envelope of the disturbing signal. Although slight shifts in biasing may be tolerated in some cases, envelope detection may result in signals within the amplifier bandwidth that cannot be distinguished from the intended signals. This adversely affects the fidelity of the intended signal transfer, and thus the signal-to-error ratio (SER). The adverse effect on the SER due to envelope detection is meant when the term EMI is used in the remainder of this paper. Note that both noise and EMI determine the total SER.

Methods to model and analyze distortion and EMI in BJTs, FETs, negative-feedback amplifiers, and also some designs of low EMI susceptible opamps have been published, e.g., [2]–[13]. A simple, systematic method to design an application specific negative-feedback amplifier with specified SER, output-, and bandwidth requirements has not been presented as yet.

Since EMI is related to nonlinear distortion, it is a function of the loop gain of the negative-feedback amplifier [11]. For a given EM environment and active device, it is therefore possible to calculate the minimum loop gain required to reduce EMI to acceptable levels without filtering. This is demonstrated by systematically designing a transimpedance amplifier for a specific EM environment. Section II presents the design specifications, including the minimally allowed SER.

In order to ensure a particular SER, the amount of disturbance the electromagnetic field generates has to be determined. Therefore, a simple method for approximating the disturbance will be presented in Section III.

TABLE I
SPECIFICATIONS

Source	Max. signal	10 μA
	Signal bandwidth	10 Hz $\cdots$ 1 MHz
	Impedance	100 kΩ // 1 pF
Load	Max. signal	1 V
	Impedance	10 kΩ // 100 pF
Transfer	Response type	Butterworth (Maximally flat pass band)
	Signal-error-ratio	$\geq$ 70 dB
EM-environment	field type	plane wave (far field)
	frequency band	1MHz$-$100MHz
	amplitude	30 V/m
	modulation depth	1

Preliminary computations showed that the bandwidth specifications could not be met with a single BJT stage due to the Miller effect. Cascode stages neutralize the adverse effect of the base–collector or gate–drain capacitance and the Miller effect does not occur. A hybrid-π model valid for both linear and second-order nonlinearity analysis of a BJT–BJT cascode stage is shown in Section IV. With the necessary changes, it can also be used to model these effects in cascode stages consisting of other combinations of active devices.

Section V demonstrates the design of a transimpedance amplifier that meets all specifications, with this BJT–BJT cascode as active part. Susceptibility measurements on the realized transimpedance amplifier are presented in Section VI, and are in close agreement with theory. Section VII presents a short discussion. Finally, Section VIII presents the concluding remarks.

II. SPECIFICATIONS

The method to design a transimpedance amplifier with a specified SER in high field strengths is demonstrated by designing such an amplifier for a given signal source and load. Table I summarizes the specifications of the source, load, signal transfer, and EM environment, respectively. All specifications chosen are realistic and may occur in practice.

The envelope of the plane waves shows low-frequency variations that are in the amplifiers' pass band. The maximum variation in the envelope corresponds to an amplitude modulation with a modulation index of 1, as stated in Table I. Such an EM environment may very well occur in practice. Industrial, scientific, and medical equipment (ISM), e.g., used for heating, diathermy, or electrosurgery, but also radio transmitters, may radiate EM fields with high field strengths and low-frequency envelope variations. In some ISM bands (13.5, 27.0, and 40.7 MHz), the amount of power that may be radiated is even unrestricted in some countries [14]. EM-field strength levels between 10 and 30 V/m can readily occur in the vicinity of these radiating equipment. Therefore, equipment in an industrial environment and life-supporting medical systems should be immune to EM fields up to at least 10 V/m [14], [15].

The consequences of a too large susceptibility in a harsh EM environment, i.e., a too low SER, of the negative-feedback amplifier (as part of a lager system) may vary from life-threatening situations in medical environments [16], [17] and in aviation, to inconvenience when telephones can be used to listen to AM radio broadcasts [1]. Maintaining a high enough SER in high EM-field strength levels is thus important, especially in possible life-threatening situations. Here, a minimal SER equal to 70 dB is expected to prevent these detrimental effects.

The relatively low upper frequency of 100 MHz to design for, has been specifically chosen. This relieves the measurement difficulties that can be expected at higher frequencies where board lay-out properties do play a significant role. The method presented in this work is, nonetheless, also applicable to much higher frequencies in the GHz range such as used by cellular phones.

We will assume that both the negative-feedback amplifier and the load are shielded from interfering fields, but the interconnect between source and amplifier will not be shielded. To ease the calculation of EM coupling, the interconnect is assumed to consist of two wires that have a fixed distance to each other, comparable with two wires of ribbon cable, and that EM interaction with the shield does not occur. We will use a so called two-wire line [18] with a length of 0.1 m, a distance between the wires of 1.27 mm, an inductance of 92.7 nH, and a measured capacitance of 2.36 pF.

The intended signal is smallest at the input of the amplifier, this is thus the place where noise and EMI have the largest detrimental effect. Both noise and EMI effects are therefore transferred to an equivalent source at the input of the amplifier.

If it is assumed that the equivalent noise power and equivalent EMI power are uncorrelated, the SER is simply the ratio of the signal power and the sum of both.

III. DETERMINING THE DISTURBING CURRENT

Using transmission line equations and by integrating the total field along the two-wire, voltages and currents at the terminals of the wire can be determined accurately [19]. These voltages and currents can also be determined for other types of interconnects, e.g., microstrip lines, with this generally valid method. For the specified frequency range, the two-wire is electrically short. Its electrical behavior may be described by means of lumped-circuit models instead of using the transmission line equations, while the induced voltage and current can be modeled by a current source in parallel with the admittances and a voltage source in series with the impedances respectively, e.g., [18].

The magnitude of the disturbing current at the input of current processing amplifiers, can easily be determined by assuming the input impedance of the amplifier, $Z_{\rm in}$, to be zero.

The practical transimpedance amplifier will not have a zero input impedance. To simplify the design process, an ideal amplifier can be considered nevertheless. Deviations in the calculated disturbing signal, due to deviations of $Z_{\rm in}$ from the ideal value, presented to the input of the amplifier can be evaluated later. If the practical transimpedance amplifier is designed properly, the constraint for the source impedance $Z_s \gg Z_{\rm in}$ still holds. The deviations between the "ideal" and "practical" values of the disturbing signal are thus expected to be small.

Under the specified conditions, the disturbing current at the input of the transimpedance amplifier can now be approximated by $i_{\rm dist,tot} = j\omega C_d dE\sin\theta$ [18], where ω is the angular frequency, C_d is the capacitance of the two-wire, d the distance between the conductors, E is the electric field strength, θ is the angle between the E-field and the two-wire, and $j = \sqrt{-1}$. When the orientation of the E-field is perpendicular to the two-

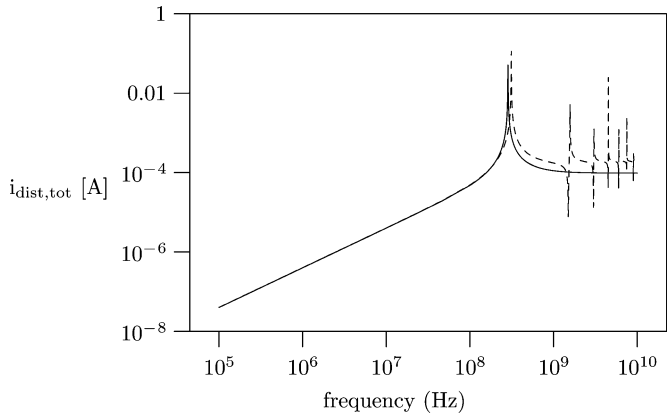

Fig. 1. Total disturbing current at the input of the transimpedance amplifier as a function of frequency calculated with a lumped-circuit model (solid line) and as predicted by transmission line theory (dashed line). At a frequency of about 240 MHz, the lumped-circuit model becomes less accurate because the two-wire is not electrically short anymore. Resonance and antiresonance points can be identified in the transmission line model based $i_{\mathrm{dist,tot}}$ calculation that do not occur in the simple model. The lumped-circuit model completely looses validity at approximately 1 GHz.

wire ($\theta = 90°$), $i_{\mathrm{dist,tot}}$ is maximal. Note that for frequencies higher than 100 MHz, the contributions of the magnetic field component and inductance L_d have to be taken into account as well.

In EMC engineering, it is customary to assume the worst case scenario, i.e., maximal field coupling. This also makes sense from a design point of view; therefore, in this paper, maximal $i_{\mathrm{dist,tot}}$ is assumed ($\theta = 90°$).

To demonstrate the validity of the lumped-circuit model for the specified maximum frequency of the interfering plane waves, Fig. 1 shows both the graph of $i_{\mathrm{dist,tot}}$ determined by the lumped-circuit model, including the magnetic field component, [18] and determined by the transmission line method [19]. Both graphs are in good agreement up to the frequency at which the lumped-circuit model becomes less accurate (≈ 240 MHz) because the two-wire is not electrically short anymore. When designing for low EMI for frequencies higher than approximately 1 GHz the transmission line method to determine $i_{\mathrm{dist,tot}}$ should be used.

IV. Modified Cascode Model

A cascode stage consists of a cascade of two transistors, a common-emitter (CE) and a common-base (CB) stage, where the CB stage is used to ensure a unilateral behavior of the CE stage.

The CB stage is a single-stage current amplifier with a current gain very close to one. Using the method presented in [11] it can be concluded that the envelope detection of the CB stage is negligible compared to that of the CE stage, even at frequencies higher than transit frequency, f_t, of the CB stage, as long as the loop gain around the CB stage is large. This large loop gain is usually easily obtained by assuring that $r_{o\mathrm{CE}} \gg r_{\pi\mathrm{CB}}, r_{o\mathrm{CB}} \gg Z_L$, and $g_{m1\mathrm{CB}} \times r_{o\mathrm{CE}} \gg \beta_{\mathrm{acCB}}$, where r_π, r_o, and β_{ac} have their usual meaning as used in the hybrid-π model and Z_L is the impedance that loads the output of the CB stage. The (linear) transconductance is denoted by g_{m1} and will be discussed in more detail later.

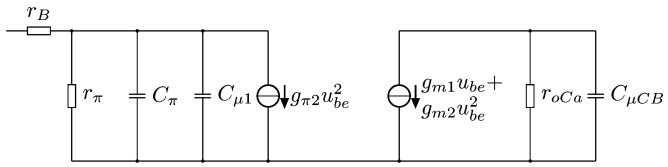

Fig. 2. Modified hybrid-π model of the BJT–BJT cascode, valid when $r_{o\mathrm{CE}} \gg r_{\pi\mathrm{CB}}, r_{o\mathrm{CB}} \gg Z_L, g_{m1\mathrm{CB}} \times r_{o\mathrm{CE}} \gg \beta_{\mathrm{acCB}}$, and valid for linear and second-order nonlinear transfer analysis.

The hybrid-π model capable of describing both linear and second-order nonlinear behavior of the cascode is shown in Fig. 2. The cascode shows an input impedance formed by base resistance r_B, base–emitter resistance r_π, and base–emitter capacitance C_π of the CE stage. In parallel with C_π there is a capacitance $C_{\mu 1} = C_{\mu\mathrm{CE}}(1 + g_{m1\mathrm{CE}}/Y_{\mathrm{inCB}})$ (Miller approximation). Y_{inCB} is the input admittance of the CB stage and equals $g_{m1\mathrm{CB}} + j\omega C_{\pi\mathrm{CB}}$. For frequencies lower than the pole in Y_{inCB}, which is approximately equal to $f_t, C_{\mu 1} = C_{\mu\mathrm{CE}}(1 + g_{m1\mathrm{CE}}/g_{m1\mathrm{CB}})$ and for frequencies higher than this pole its value reduces to $C_{\mu 1} \approx C_{\mu\mathrm{CE}}$. The output is formed by a resistance, r_{oCa}, approximately equal to $\beta_{\mathrm{acCB}} \times r_{o\mathrm{CB}}$, shunted by a capacitance equal to $C_{\mu\mathrm{CB}}$.

At the input, a voltage controlled current source of value $g_{\pi 2}u_{be}^2$ represents the second-order nonlinearity of the base current due to the nonlinear input conductance. Finally, at the output there is also a voltage controlled current source of value $g_{m1}u_{be} + g_{m2}u_{be}^2$ that represents the linear and second-order nonlinear term of the collector current due to the exponential input voltage to output current relation of the BJT. g_{m1}, g_{m2}, and $g_{\pi 2}$ can be determined by a Taylor expansion in the BJT operating point [2], [6], [7], [11].

The expressions for g_{m1} and g_{m2} are thus given by

$$g_{m1} = \frac{q}{n_f kT} I_{cQ}, \qquad \text{in amperes per volt} \tag{1}$$

$$g_{m2} = \frac{1}{2}\left(\frac{q}{n_f kT}\right)^2 \cdot I_{cQ} = \frac{1}{2}\frac{q}{n_f kT} g_{m1}, \qquad \text{in amperes per volt squared} \tag{2}$$

where I_{cQ} is the bias current, k is Boltzmann's constant, T is the absolute temperature in Kelvin, q is the electron charge, and n_f is the forward emission coefficient, usually close to 1.

In the so-called midcurrent region the current gain β_{ac} is virtually constant, because secondary nonlinear effects due to both low (recombination in the base–emitter depletion layer) and high bias current (nonnegligible injection of minority carriers in the base) operation are negligible [20], [21]. The distortion behavior of the BJT is minimal in this case.

A Taylor expansion of the nonlinear relation of the base current and the base–emitter voltage in the midcurrent region results in

$$g_{\pi 2} = \frac{1}{2}\frac{d^2}{dU_{be}^2} I_b(U_{be}) = \frac{1}{2}\left(\frac{q}{n_f kT}\right)^2 \cdot \frac{I_{cQ}}{\beta_{\mathrm{ac}}} = \frac{g_{m2}}{\beta_{\mathrm{ac}}}, \qquad \text{in amperes per volt square.} \tag{3}$$

After some straightforward mathematical manipulation of the Gummel–Poon equations [20], the lower and upper boundaries of the midcurrent region can be determined from

$$U_{beQ\min} = \frac{kT}{q}\frac{n_f n_e}{n_f - n_e}\ln\left(\frac{1}{b\beta_f}\frac{I_s}{I_{se}}\right) \tag{4}$$

$$U_{beQ\max} = \frac{n_f kT}{q}\ln\left(\frac{cI_{KF}}{4I_s}\right) \tag{5}$$

where I_s is the saturation current, n_e is the base–emitter leakage coefficient, β_f is the forward current amplification factor, I_{se} is base–emitter leakage current, and I_{KF} is the forward current value where the current gain drops to half its value [20]. Coefficient b presents a boundary value for the maximal contribution of the base–emitter leakage current to the base current, while coefficient c presents the maximal contribution of I_{KF} to the collector current. Values of $b = 20$ and $c = 0.1$ usually result in negligible secondary nonlinear effects and therefore seem to be reasonable. The results of (4) and (5) can be used to easily obtain the boundary values of I_{cQ}.

Truncating a Taylor expansion after the second term introduces inaccuracy. However, for values of signal voltage $\hat{u}_{be}$ up to 10 mV the inaccuracy of the resulting signal current $\hat{i}_c$ is smaller than 1% [11]. C_π depends on I_{cQ} and is therefore also nonlinear. The resulting nonlinear current $i_{c\pi}$ is, however, proportional to $\omega_l C_{\pi 2}\hat{u}_{be}^2$. $C_{\pi 2}$ represents the second-order nonlinear value of C_π and ω_l is the low-frequency variation of the envelope. Current $i_{c\pi}$ is often negligibly small compared to the currents at ω_l due to $g_{\pi 2}$, respectively, g_{m2}. C_π may therefore be regarded as being constant. $C_{\mu 1}$ is a constant because its value is determined by a junction capacitance which is only slightly dependent on $\hat{u}_{be}$. The junction capacitance $C_{\mu\mathrm{CB}}$ may have considerable signal voltage across it, modulating its capacitance value. It is, however, usually loaded by the input impedance of a subsequent stage or load, that is much smaller than $1/j\omega C_{\mu\mathrm{CB}}$, making its (nonlinear) effect negligible.

In properly designed negative-feedback amplifiers $\hat{u}_{be}$ will be most probably below 10 mV. Therefore, the modified hybrid-π model of Fig. 2 can be used to analyze linear and second-order nonlinear, EMI, behavior.

The combined action of the voltage controlled current sources tend to reduce the second-order nonlinear behavior. This linearizing action is especially effective when signal source resistance R_s is much larger than r_π [3], see Section V, (13).

V. Design Method

The design of an application-specific negative-feedback amplifier can be divided in several orthogonal steps [22]. From the source and load specifications the required transfer and feedback configuration is determined first. Second, the noise properties are investigated, which result in optimal bias requirements. Third, the output requirements to the load are determined. As fourth step, the required loop gain and g_{m1} are determined to meet the EMI specification. The fifth step is estimating the bandwidth and applying frequency compensation to achieve a Butterworth (maximally flat) characteristic. Finally, as sixth step the biasing arrangement is designed.

From the source and load specifications (see Table I), it follows that the transimpedance should have a 100 kΩ value to realize 1 V across the load for a source current of 10 μA. This transimpedance can, e.g., be implemented by a negative-feedback amplifier with a feedback resistor of 100 kΩ.

Since noise will always be generated, thus also when there is no interference, it will determine the maximal obtainable SER and is therefore considered before EMI. The maximal allowable EMI now follows from the required SER and the noise behavior. Noise and EMI are extensively dealt with in the next sections.

For elaborate treatment of the other steps we refer to [22]. They are only briefly discussed here.

A. Noise

Under the assumption that the signal source generates noise equivalent to the thermal noise of the real part of its admittance, for the transimpedance amplifier with a bipolar input stage the equivalent input noise power is given by

$$\begin{aligned}\overline{i_{n,\mathrm{eq}}^2} = 4kTf_h\Bigg\{&\frac{1}{R_s}+\frac{1}{R_t}+\left(r_B+\frac{1}{2g_{m1}}\right)\\ &\times\left[\left(\frac{1}{R_s}+\frac{1}{R_t}\right)^2+\frac{1}{3}(2\pi f_h C_x)^2\right]\\ &+\frac{g_{m1}}{2\beta_{\mathrm{dc}}}\left[\left(1+r_B\left(\frac{1}{R_s}+\frac{1}{R_t}\right)\right)^2\right.\\ &\left.+\frac{1}{3}(r_B 2\pi f_h C_x)^2\right]\Bigg\}.\end{aligned} \tag{6}$$

In this equation, f_h is the upper frequency of the bandwidth. Because of the required large bandwidth of 1 MHz the influence of the lower frequency corner of the bandwidth and the influence of flicker noise can be neglected, since for modern BJTs the frequency at which the flicker noise equals the white noise is usually a few Hz [22]. Further, R_s is the source resistance, C_x is formed by the source capacitance C_s, and the capacitance of the two-wire C_d, in parallel. R_t is the feedback resistor, r_B is the base resistance, and β_{dc} is the dc current gain of the transistor.

For low noise power, it immediately follows from (6) that a BJT should be used having a high value of β_{dc} and, preferably, a low value of r_B. Also, (6) is valid under the assumption that current noise contribution of the BJT is dominated by the base current. This is allowed when $\beta_{\mathrm{ac}} \gg 1$ and $f_h \ll f_t/\sqrt{\beta_{\mathrm{ac}}}$ [22], f_t being the transit frequency; conditions that usually can be met easily.

B. Calculation of the Required Transconductance

When we design for equal contributions of both noise power and EMI power to the SER, the most optimal design regarding the SER results. After all, when a lot design effort is put in low noise design while EMI dominates the SER, this effort is wasted. Similarly, design effort and power is wasted when EMI is designed to be much lower than the noise. Therefore, EMI should have at most the same order of magnitude as the noise. From this maximum EMI power, the minimal required transconductance of the active part is determined.

The disturbing current generated by the nonconstant envelope interfering EM field, shows the same amplitude variations

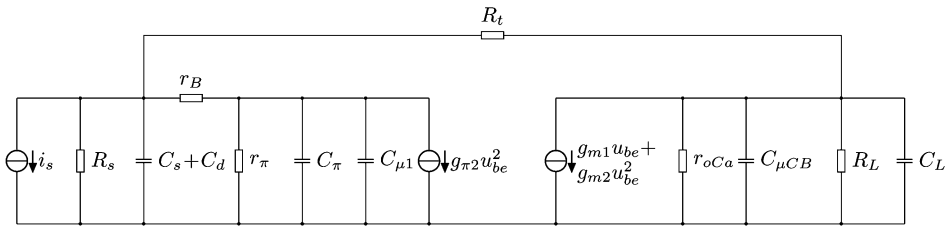

Fig. 3. Hybrid-π signal diagram of the transimpedance amplifier.

as the EM field. Like noise, the resulting envelope detection (EMI) caused by the disturbing current can be represented by one equivalent current source at the input of the negative-feedback amplifier. This source is given by [11]:

$$i_{s,\mathrm{env}}(\omega_c) = i_{\mathrm{dist,tot}}(\omega_c)^2 \chi(\omega_c)^2 m D_2 \frac{1}{\xi_{\omega_l}}. \tag{7}$$

The angular frequency of the disturbing current is ω_c. χ is the transfer from the disturbing current to the input of the BJT, i.e., the transfer from $i_{\mathrm{disturb,tot}}$ to u_{be}. ξ_{ω_l} is the low-frequency term of the transfer from signal source i_s to u_{be} and m is the modulation depth. For a transimpedance amplifier ξ_{ω_l} also determines the transfer from source ${g_{\pi 2}u_{be}}^2$ to u_{be}, when $r_B \ll R_s//(R_t + R_L)$. D_2 is the second-order nonlinearity term, which is a measure for the second-order nonlinear behavior of the negative-feedback amplifier. Here, $D_2 = g_{m2}/g_{m1} - g_{\pi 2}\xi_{\omega_l}$.

Fig. 3 depicts the hybrid-π diagram of the transimpedance amplifier. Although the exact values of the circuit elements of the cascode are not yet known, using Table I some conclusions can be drawn: load capacitance C_L will most probably be much larger than $C_{\mu\mathrm{CB}}, C_\pi, C_{\mu 1}$ and $C_s + C_d$. There will be two poles determining the bandwidth, with pole p_L affected by C_L and R_L located at a lower frequency than pole p_i affected by the input capacitance formed by $C_\pi, C_{\mu 1}, C_s + C_d$, and R_s shunted by R_t and r_π. Expressions for the poles will be given later.

Transfer $\xi(\omega_c)$ will have a zero located at approximately the same frequency as p_L, and therefore, shows a single pole transfer [11]. The loop gain often shows two dominant poles in case of application specific amplifiers. $\chi(\omega_c)$ is given by the ratio of $\xi(\omega_c)$ and the loop gain and, when $\omega_c > |p_L|$, it will increase with increasing frequency up to some maximum value at $\omega_{\max}$ after which it will decrease again [11], as Fig. 4 shows. As a result, $i_{s,\mathrm{env}}$ will show the same behavior.

Fig. 4 shows the transfer $\chi(\omega_c)$, current $i_{\mathrm{dist,tot}}(\omega_c)$ and the resulting equivalent envelope detection source $i_{s,\mathrm{env}}(\omega_c)$ in one figure. It shows how the slopes of $i_{s,\mathrm{env}}(\omega_c)$ depend on $i_{\mathrm{dist,tot}}(\omega_c)$ and the slopes of $\chi(\omega_c)$. Between $|p_l|$ and $\omega_{\max}, i_{s,\mathrm{env}}$ increases with a slope of 80 dB/dec and it stabilizes at a constant value for frequencies higher than $\omega_{\max}$. Further, $\omega_{\max}$ will occur near the upper corner frequency of the bandwidth ω_0 given by the square root of the loop gain poles product (LP). LP equals $p_L p_i(1 - A\beta_0)$ and $A\beta_0$ is the loop gain. Note that the flat region of $|i_{s,\mathrm{env}}|$ is due to out-of-band disturbance and thus the region of interest.

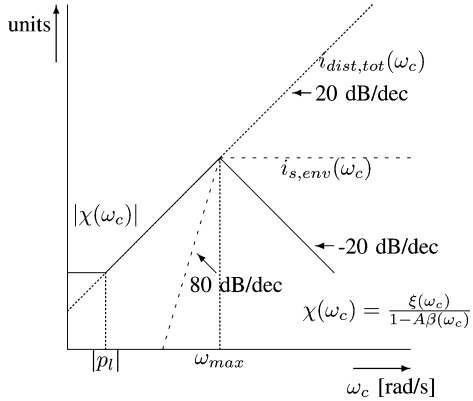

Fig. 4. Transfers $|\chi|$ (solid line), $|i_{\mathrm{dist,tot}}|$ (dotted line), and $|i_{s,\mathrm{env}}|$ (dashed line) as a function of frequency. The maximum frequency used in this figure is in the "differentiating" region of $i_{\mathrm{dist,tot}}$. Note that the flat region of $|i_{s,\mathrm{env}}|$ is due to out-of-band disturbance and thus the region of interest.

Transfer $\chi(s)$ is given by [11]

$$\chi(s) = \xi_0 \frac{p_L p_i\,(1-(s/p_L))}{s^2 - s\,(p_L + p_i - A\beta_0(p_L p_i/z_\beta)) + p_L p_i(1 - A\beta_0)} \tag{8}$$

where ξ_0 is the zero-frequency value of the load that current source i_s experiences. Further, there is a term $-A\beta_0(p_L p_i)/(z_\beta)$ that increases the damping factor ζ, given by $\zeta = (-(p_L + p_i - A\beta_0(p_l p_i)/(z_\beta)))/(2\omega_0)$, with z_β being a phantom zero introduced by the designer to manipulate the poles into the desired positions for the required frequency response of the source to load transfer, the transimpedance in this case. $\zeta = (1/2)\sqrt{2}$ is chosen to obtain a Butterworth transfer. For values of ζ smaller than $(1/2)\sqrt{2}$, overshoot will occur at the upper edge of the bandwidth in both the source to load transfer and $\chi(\omega)$. Proper frequency compensation thus reduces EMI susceptibility near the upper edge of the bandwidth.

The maximum value of $\chi_{\max}$ occurs at a frequency approximately equal to the upper limit of the bandwidth, ω_0. Using this approximation and (8) (disregarding the phantom zero term for the time being), the maximum value is derived to be

$$\chi_{\max} \approx \frac{\chi_0}{2\zeta}\sqrt{\frac{\omega_0^2 + p_L^2}{p_L^2}}. \tag{9}$$

Still, χ_0, ξ_0 and $A\beta_0$ are unknown. To come to an equation that can be solved, Fig. 3 has to be considered.

Output resistance $r_{o,CA}$ can be expected to have a value much greater than R_L and can therefore be neglected. For now, it is assumed that r_B can be neglected because it is much smaller than r_π. When this is not the case, its effect can be evaluated in a later stadium. Feedback factor β_0 is determined from Fig. 3 and $A = g_{m1}$. With $r_\pi = (\beta_{\rm ac})/(g_{m1})$ it follows for the loop gain

$$A\beta_0 = -\beta_{\rm ac}\frac{R_s R_L}{r_\pi R_s + (r_\pi + R_s)(R_L + R_t)}. \tag{10}$$

Also, from Fig. 3 follows directly for ξ_0

$$\xi_0 = \frac{r_\pi R_s(R_t + R_L)}{R_s(r_\pi + R_t + R_L) + r_\pi(R_t + R_L)}. \tag{11}$$

Equation (8) shows that $\chi_0 \approx \xi_0/(-A\beta_0)$ when $-A\beta_0 \gg 1$. It is now possible to simplify this expression to a form where, apart from g_{m1}, no hybrid-π parameters appear.

$$\chi_0 \approx \frac{R_t + R_L}{R_L}\frac{1}{g_{m1}}. \tag{12}$$

Envelope variations usually occur at a low frequency. As an approximation, $\xi_{\omega_l} \approx \xi_0$ in (7) can be used. For D_2 can now be derived to hold

$$D_2 = \frac{q}{2n_f kT}\frac{1}{1 + \frac{R_v}{r_\pi}} = \frac{q}{2n_f kT}\frac{\beta_{\rm ac}}{\beta_{\rm ac} + g_{m1}R_v} \tag{13}$$

and $R_v = R_s//(R_t + R_L)$. Note that D_2 may become small when the BJT is current driven, i.e., $R_v \gg r_\pi$, and reaches a maximal value of $q/(2n_f kT)$ under voltage drive condition: $R_v \ll r_\pi$.

Combining the expression for ζ, with the phantom zero disregarded, (7), (9), (12), and (13) and solving for g_{m1} results in

$$g_{m1} = \frac{-\beta_{\rm ac}}{2R_v} + \frac{1}{2i_{s,\rm env}R_v}\sqrt{i_{s,\rm env}\beta_{\rm ac}(i_{s,\rm env}\beta_{\rm ac} + 4E)}$$
$$E = i^2_{\rm dist,tot}R_v m\frac{R_t + R_L}{R_L}\left(\frac{p_i}{p_l}\right)\frac{\omega_0^2 + p_L^2}{(p_L + p_i)^2}\frac{q}{2n_f kT}. \tag{14}$$

The required transconductance can be calculated from this equation if one uses the desired bandwidth as the value for ω_0 and a first-order approximation for p_L and p_i. This first-order approximation for p_L follows from Fig. 3 by neglecting the influence of r_π, which is allowed because the shunt $r_\pi//R_s$ is in series with the large-valued resistor R_t, and is $p_L \approx -1/(R_L C_L)((R_L + R_t))/(R_t)$. Under the condition that R_s and R_t are much larger than r_π and C_π is larger than $C_x, p_i \approx -\omega_t/\beta_{\rm ac}$. Pole p_i thus follows from the transistor properties. As a first-order approximation of $\beta_{\rm ac}$, the maximal forward current gain β_f, as specified in Spice models, can be used.

C. Design of the BJT Transimpedance Amplifier

To quickly realize a prototype transimpedance amplifier, it was chosen to design and build it using discrete BJTs. From the large amount of BJTs that satisfy the design constraints, the BC548B, an npn transistor, was chosen.

1) Noise Calculation: From the noise equation derived earlier (6), the optimal bias current for the transistor is determined to be approximately 10 μA for the BC548B. The noise contribution of the BJT is virtually negligible compared to the noise contribution of R_s and R_t. The resulting equivalent noise power is $\overline{i^2_{n,\rm eq}} = 354 \times 10^{-21}\,\mathrm{A}^2$. The resulting SNR is 84.5 dB, which is the maximal obtainable SER.

2) Output Capability: In order to deliver a signal of 1 V peak to the load, a current of 637 μA is required. When this current has to be delivered to the load, one has to make sure that enough current keeps flowing through the output stage to avoid unacceptable decrease in transit frequency f_t. Biasing the output stage at approximately 1.5 times the current to be delivered is a good strategy [22], resulting in a minimal bias current of 1 mA.

3) EMI: To be on the safe side, to compensate for component spread and uncertainties in the exact value of $i_{\rm dist,tot}$, the SER to design for can be taken 73 dB, so there is a margin of 3 dB. With a SER $=$ 73 dB the total equivalent input error power equals $i^2_{n,\rm eq} + i^2_{s,\rm env} = 5 \times 10^{-18}$ A^2. If it is assumed that both components equally contribute to the "error power", a value for $i_{s,\rm env}$ of 1.58 nA is obtained.

It follows from $i_{\rm dist,tot} = j\omega C_d dE$ that at ω_0 the allowed maximal value of $i_{\rm dist,tot}$ is 567 nA. However, to be on the safe side again, a bandwidth of 1.1 MHz is designed for. Using (14) with the corresponding $i_{\rm dist,tot}$ of 621 nA, it is now found that g_{m1} should have a value of 48.5 mA/V, which corresponds to an I_{cQ} of 1.3 mA, to satisfy the EMI demands. This value of I_{cQ} is located in the midcurrent region. A β_f of 294 and an ω_t of 628 M rad/s followed for the BC548B.

4) Discussion: The I_{cQ} determined from the above EMI considerations is only a little higher than required for the output capability. The power consumption thus does not excessively increase. There is, however, a large discrepancy between the values of I_{cQ} for minimal noise performance and required for EMI performance.

Biasing the cascode at a current of 1.3 mA instead of 10 μA changes the noise behavior of the BJT. The contribution of the BJT to the equivalent noise power increases and will now be of the same order of magnitude as the noise from R_s and R_t, which is still acceptable. The equivalent noise current power is $\overline{i^2_{n,\rm eq}} = 1.94 \times 10^{-18}\mathrm{A}^2$, resulting in a SER of 73.5 dB.

5) SER Analysis and Amplifier Implementation: Biasing the BJT cascode at a collector current I_{cQ} of 1.3 mA and a collector–emitter voltage of 2 V results in the values of the modified hybrid-π parameters tabulated in Table II. They were determined using Pspice to determine the linear values and (2) and (3) to determine the second-order values of the modified hybrid-π model. The simulated value of g_{m1} is slightly larger than the value obtained with (1). This is because the calculated I_{cQ} of 1.3 mA is a rounded up value.

TABLE II
HYBRID-π PARAMETERS, $I_{cQ} = 1.3$ mA, $U_{ceQ} = 2$ V

r_B = 26.5 Ω	β_{ac}= 286
r_π =5.79 kΩ	r_o=48k4 Ω
$g_{\pi 2}$ =3.30 mA/V^2	C_π =70.2 pF
g_{m1} =49.3 mA/V	C_μ =2.4 pF
g_{m2} =945 mA/V^2	f_t =108 MHz

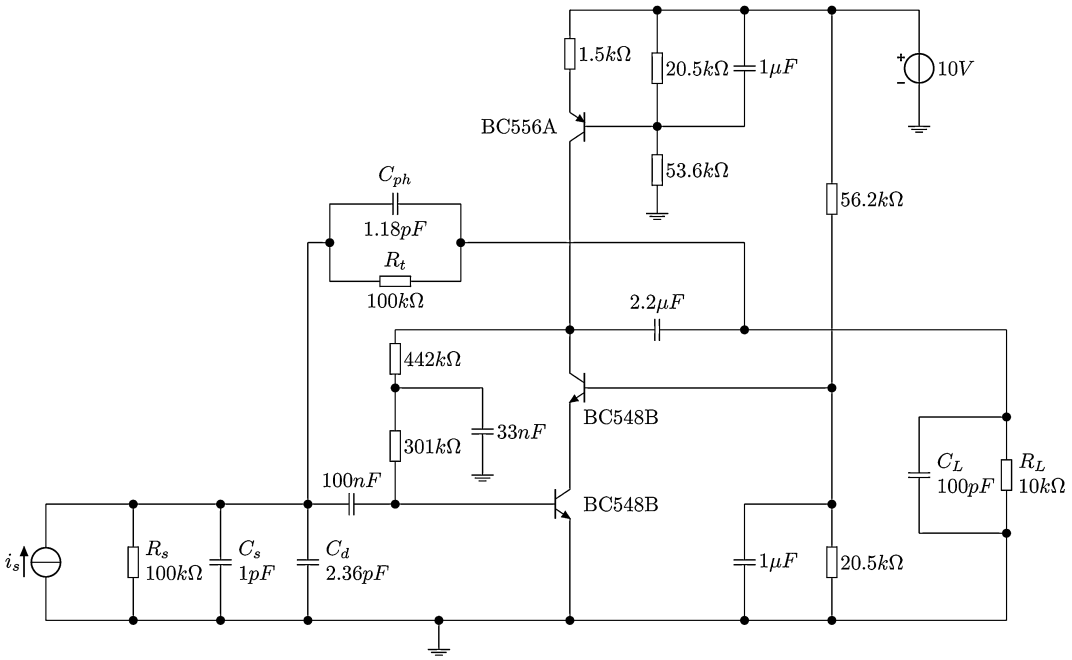

Fig. 5. Schematic of the transimpedance amplifier.

The loop gain is equal to -23.4, which results in an accuracy of the transimpedance of 99.6 dB[Ω]; just 0.4 dB[Ω] less than in the ideal case. Poles p_L and p_i can be found at -1.06×10^6 rad/s, respectively, -2.54×10^6 rad/s. The bandwidth ω_0, as predicted by the LP, is 8.13×10^6 rad/s (1.29 MHz) and $\zeta = 0.22$. Note that the bandwidth specifications can not be met with a noncascode single stage. Due to the Miller effect the bandwidth is in this case limited to approximately 460 kHz.

$\chi_{\max}$ reaches a high value at approximately ω_0 due to the low value of ζ. The minimal SER to be expected near ω_0 amounts 70 dB, which is just within specifications. After frequency compensation to obtain a Butterworth characteristic, however, no overshoot will occur and therefore $\chi_{\max}$ will decrease, resulting in a larger SER.

For a Butterworth characteristic a phantom zero [22] was introduced by shunting R_t with a capacitance C_{ph} of 1.18 pF. Now, we have: $\zeta = 0.69$ and $\omega_{\max} = 8.07 \times 10^6$ rad/s, which is indeed very close to $\omega_0 = 8.13 \times 10^6$ rad/s.

$\chi_{\max}$ is determined to be 1211 Ω. This results in a corresponding value of $i_{s,\mathrm{env}} = 224$ pA at ω_0. For frequencies just above ω_0, the slope of $\chi(\omega_c)$ (see Fig. 4) has not reached -20 dB/dec yet. This slope is reached after approximately an octave. In the frequency band $\omega_0 - 2\omega_0, \chi(\omega_c)$ decreases about 3 dB and $i_{\mathrm{dist,tot}}$ increases 6 dB, resulting in an increase of 6 dB in $i_{s,\mathrm{env}}$. As a result, $i_{s,\mathrm{env}} \approx 450$ pA for frequencies larger than $2\omega_0$. The SER to be expected thus equals 76.1 dB.

The required SER is easily reached after frequency compensation. The designer could consider to reduce the I_{cQ} a little in order to reduce power consumption. As a consequence $i_{s,\mathrm{env}}$ will increase and $i_{n,\mathrm{eq}}$ will decrease, but the required SER can still be reached. A trade-off between power consumption and SER is thus possible. We will not elaborate on this here.

Fig. 5 shows the final schematic of the designed transimpedance amplifier. A current source realized with a BC556A pnp BJT biases the cascode at a collector current of 1.3 mA. The resistors required for establishing the desired base–emitter and collector–emitter voltages are chosen such that LP of the transimpedance is virtually not reduced. Spice simulations show a transimpedance of 99.6 dB[Ω], a bandwidth of 1.29 MHz (8.11×10^6 rad/s) and an $i_{n,\mathrm{eq}}$ of 1.55 nA. These figures are very close to the calculated values.

The effects of the nonzero input impedance of the transimpedance amplifier on $i_{\mathrm{dist,tot}}$ can now be evaluated. As stated before, the effect is expected to be minor; the inaccuracy of the amplifier transfer function is just 0.4 dB[Ω]. Such a low value of the inaccuracy implies an input impedance much smaller than the impedance formed by Z_s and the two-wire.

Using the accurate transmission line equations, the effect of the nonzero input impedance has been evaluated. It was found that over the frequency range of interest the accuracy of the approximated value of $i_{\mathrm{dist,tot}}$ is within 90%, which is acceptable.

VI. Measurements

The transimpedance amplifier as depicted in Fig. 5 has been built and tested. The transimpedance was measured to be 99.6 dB[Ω] and the bandwidth 1.1 MHz. Compensation is realized by a C_{ph} of 1 pF. It should be noted that due to component spread in C_{ph} and the parasitic capacitance of R_t, the actual total compensation capacitance was approximately 1.6 pF. This was accounted for in the calculation of $i_{s,\mathrm{env}}$ in Fig. 6.

Generating an EM plane wave of 30 V/m and to make also sure that just this plane wave is picked up by the transimpedance amplifier, may be a tedious task. As shown in Section III, the disturbance current is dominated by a capacitance and the electric field component. Therefore, it was chosen to capacitively couple the disturbing signal to the amplifier. Besides, simulating field to wire coupling by coupling an equivalent signal via a conductance to the amplifier, is a valid and generally used method for frequencies at which transmission line effects are minimal [23].

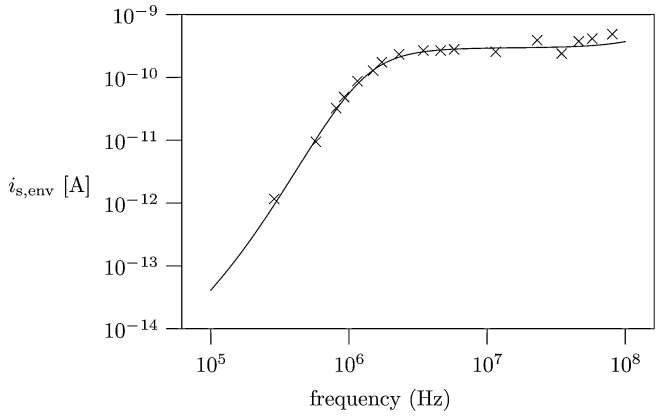

Fig. 6. Amplitude of the equivalent envelope detection source at the input of the amplifier as a function of frequency. The line is calculated. The crosses are actual measurements. The amplifier is frequency compensated to obtain a Butterworth characteristic. Note that the out-of-band measurements of interest are located above 1 MHz. The in-band detection components are only shown for completeness.

The electric field component has been replaced by a voltage from a signal generator and the capacitance by a coupling capacitor equal to the capacitance of the, removed, two-wire. The voltage was chosen such that at 1 MHz i_{dist} amounted to the required 567 nA. Due to the differentiating character of the coupling capacitance i_{dist} will increase with increasing frequency.

The measured and calculated values of $i_{s,\mathrm{env}}$ are shown in Fig. 6. The measured values are in close agreement with the calculations and, as expected, no overshoot appears both in calculation and in measurement. Note that the out-of-band measurements of interest are located above 1 MHz. The in-band detection components are only shown for completeness.

The calculated equivalent current $i_{s,\mathrm{env}}$ flattens out at a maximum value of approximately 428 pA. This is close to the approximated value of 450 pA.

VII. Discussion

This amplifier was designed to meet a certain SER specification for interfering fields up to 100 MHz. That does not imply that there are no other design solutions and not even that this is the best one possible. It can, e.g., be expected that both noise and EMI requirements can be met by a (CMOS) FET implementation of the amplifier also. Probably, however, a more complicated, multistage solution will be required to meet the bandwidth specification due to the often too low LP of a single stage FET (cascode) implementation.

Here, we have chosen to demonstrate that with enough loop gain severe EMI requirements can be met with a BJT cascode, that is stronger nonlinear than a FET (cascode).

Extending the specification for the interference from 100 MHz to 1 GHz or higher, two extra effects have to be taken into account in the design process. First, transmission line theory shows resonances in $i_{\mathrm{dist,tot}}$ at frequencies higher than 1 GHz. Second, r_B and $C_s + C_d + C_{ph}$ (in series with $C_\pi + C_{\mu 1}$) will introduce a nondominant pole in $\chi(\omega_c)$ at approximately 1.4 GHz. Its effect on the disturbance is that of a first-order low-pass filter. High-frequency maxima will thus be attenuated, leaving the maximum at ca. 340 MHz as the EMI determining value of $i_{\mathrm{dist,tot}}$. A new, higher value, of g_{m1}, and hence, $A\beta_0$, will be needed. It could be that now our simple cascode amplifier can not meet the specifications and a different implementation is required.

VIII. Conclusion

In this paper, a systematic method to design a transimpedance amplifier with specified EMI behavior has been presented. It makes use of a simple method to approximate the amount of disturbing signal at the input of a negative-feedback amplifier due to an interfering EM plane wave, and also of a modified hybrid-π model that can be used for calculation of both linear and second-order transfers of a bipolar junction transistor cascode.

Using the design method, the required transconductance to reach the specifications can be calculated, from which the biasing of the cascode follows.

The transimpedance amplifier has been designed to have a transimpedance of 100 kΩ, a bandwidth of 1 MHz, and a minimal signal-to-error ratio of 70 dB, resulting from both noise and interference, while being subjected to a plane wave of 30 V/m.

The transimpedance amplifier has been built. Measurements are in good agreement with calculations and simulations, and thus, support the method presented in this paper.

References

[1] J. J. Goedbloed, "Kluwer technische boeken," in *Elektromagnetische Compatibiliteit*, 3rd ed. Englewood Cliffs, NJ: Prentice Hall, 1993.

[2] D. D. Weiner and J. F. Spina, *Sinusoidal Analysis and Modeling of Weakly Nonlinear Circuits, With Applications to Nonlinear Effects*. New York: Van Nostrand/Reinhold, 1980.

[3] E. K. de Lange, A. van Staveren, O. De Feo, F. L. Neerhoff, M. Hasler, and J. R. Long, "Predicting nonlinear distortion in common-emitter stages for amplifier design using volterra series," in *Proc. NDES*, 2002, pp. 41–44.

[4] R. van Langevelde and F. M. Klaassen, "Effect of gate-field dependent mobility degradation on distortion analysis in mosfets," *IEEE Trans. Electron Devices*, vol. 44, no. 11, pp. 2044–2052, Nov. 1997.

[5] R. van Langevelde and F. M. Klaassen, "Accurate drain conductance modeling for distortion analysis in mosfets," in *Proc. Int. Electron Devices Meet.*, 1997, pp. 313–316.

[6] W. Sansen, "Distortion in elementary transistor circuits," *IEEE Trans. Circuits Syst. II, Analog Digit. Signal Process.*, vol. 46, no. 3, pp. 315–325, Mar. 1999.

[7] P. Wambacq, G. G. E. Gielen, P. R. Kinget, and W. Sansen, "High-frequency distortion analysis of analog integrated circuits," *IEEE Trans. Circuits Syst. II, Analog Digit. Signal Process.*, vol. 46, no. 3, pp. 335–345, Mar. 1999.

[8] F. Fiori and P. S. Crovetti, "Nonlinear effects of radio-frequency interference in operational amplifiers," *IEEE Trans. Circuits Syst. I, Fundam. Theory Appl.*, vol. 49, no. 3, pp. 367–372, Mar. 2002.

[9] S. Graffi, G. Masetti, and D. Golzio, "New macromodels and measurements for the analysis of EMI effects in 741 op-amp circuits," *IEEE Trans. Electomagn. Compat.*, vol. 33, no. 1, pp. 25–33, Feb. 1991.

[10] E. D. Totev and C. J. M. Verhoeven, "Design considerations for lowering sensitivity to out of band interference of negative-feedback amplifiers," in *Proc. ISCAS*, 2005, vol. 2, pp. 1597–1600.

[11] M. J. van der Horst, A. C. Linnenbank, and A. van Staveren, "Amplitude-modulation detection in single-stage negative-feedback amplifiers due to interfering out-of-band signals," *IEEE Trans. Electromagn. Compat.*, vol. 47, no. 1, pp. 34–44, Feb. 2005.

[12] J. M. Redouté and M. Steyaert, "EMI resistant CMOS differential input stages," *IEEE Trans. Circuits Syst. I, Reg. Papers*, vol. 57, no. 2, pp. 323–331, Feb. 2010.

[13] A. Richelli, L. Colalongo, M. Quarantelli, and Z. M. Kovacs-Vajna, "Robust design of low EMI susceptibility CMOS opamp," *IEEE Trans. Electromagn. Compat.*, vol. 46, no. 2, pp. 291–298, May 2004.

[14] Cenelec, Limits and methods of measurement of radio disturbance characteristics of industrial, scientific and medical (ISM) radio-frequency equipment Cenelec, Brussels, Belgium, NEN-EN 55011, 1992.

[15] "Medical Electrical Equipment, Part 1," IEC 601-1-2, 1993.

[16] "Radiofrequency interference with medical devices," *IEEE Eng. Med. Biol. Mag.*, vol. 17, no. 3, pp. 111–114, May/Jun. 1998, IEEE.
[17] P. S. Ruggera and E. R. O'Bryan, "Studies of apnea monitor radiofrequency electromagnetic interference," in *Proc. Annu. Int. Conf. IEEE Eng. Med. Biol. Soc.*, 1991, pp. 1641–1643.
[18] C. R. Paul, *Introduction to Electromagnetic Compatibility*, 1st ed. New York: Wiley, 1992.
[19] A. A. Smith, *Coupling of External Electromagnetic Fields to Transmission Lines*, 1st ed. New York: Wiley, 1977.
[20] I. E. Getreu, *Modelling the Bipolar Transistor*, 1st ed. Amsterdam, The Netherlands: Elsevier, 1978.
[21] P. R. Gray, P. J. Hurst, S. H. Lewis, and R. G. Meyer, *Analysis and Design of Analog Integrated Circuits*, 4th ed. New York: Wiley, 2001.
[22] C. J. M. Verhoeven, A. van Staveren, G. L. E. Monna, M. H. L. Kouwenhoven, and E. Yildiz, *Structured Electronic Design, Negative-Feedback Amplifiers*, 1st ed. Norwell, MA: Kluwer, 2003.
[23] K. Javor, "On field-to-wire coupling versus conducted injection techniques," in *Proc. IEEE Int. Symp. EMC*, 1997, pp. 479–487.

Marcel J. van der Horst received the Ing. degree in electrical engineering from the Hogeschool van Amsterdam, Amsterdam, The Netherlands. He is currently working toward the Ph.D. degree from the Delft University of Technology, Delft, The Netherlands.

From 1995 to 2008, he was a designer of biomedical instrumentation at the Academic Medical Center, Amsterdam. He is currently a Lecturer with the Hogeschool van Amsterdam.

André C. Linnenbank (M'09) received the M.Sc. degree in physics and the Ph.D. degree from the University of Amsterdam, Amsterdam, The Netherlands, in 1989 and 1996, respectively.

From 1989 to 2000, he was with the Medical Physics Department, Academic Medical Center, Amsterdam, where he has been he has been in the Clinical and Experimental Cardiology Department since 2000. His current research interests include cardiac arrhythmia, multichannel ECG recordings, medical imaging modalities, and signal and image processing.

Wouter A. Serdijn (SM'08) was born in Zoetermeer, The Netherlands, in 1966. He received the "ingenieurs" M.Sc. degree from the Faculty of Electrical Engineering, Delft University of Technology, Delft, The Netherlands, in 1989, and the Ph.D. degree from the Electronics Research Laboratory, Delft University of Technology, in 1994.

He is currently with the Delft University of Technology. He is a coeditor and coauthor of the books *Ultra Low-Power Biomedical Signal Processing: An Analog Wavelet Filter Approach for Pacemakers* (Springer, 2009), *Circuits and Systems for Future Generations of Wireless Communications* (Springer, 2009), *Power Aware Architecting for Data Dominated Applications* (Springer, 2007), *Adaptive Low-Power Circuits for Wireless Communications* (Springer, 2006), *Research Perspectives on Dynamic Translinear and Log-Domain Circuits* (Kluwer, 2000), *Dynamic Translinear and Log-Domain Circuits* (Kluwer, 1998), and *Low-Voltage Low-Power Analog Integrated Circuits* (Kluwer, 1995). He has authored or coauthored six book chapters, and more than 200 publications and presentations. He is engaged in teaching analog electronics, analog signal processing, micropower analog IC design, and electronic design techniques. His current research interests include low-voltage, ultralow-power, high-frequency, and dynamic-translinear analog ICs along with circuits for RF and ultra-wideband (UWB) wireless communications, cochlear implants, portable, wearable, implantable, and injectable ExG recorders and pacemakers.

Dr. Serdijn is a mentor of the IEEE. He has received the EE Best Teacher Award in 2001 and 2004. He was an Associate Editor for the IEEE TRANSACTIONS ON CIRCUITS AND SYSTEMS—I: REGULAR PAPERS (2004–2005) and the IEEE TRANSACTIONS ON CIRCUITS AND SYSTEMS—II: EXPRESS BRIEFS (2002–2003 and 2006–2007), a Tutorial Session Cochair for the IEEE International Symposium on Circuits and Systems (ISCAS) 2003, a Analog Signal Processing Track Cochair for ISCAS 2004 and ISCAS 2005, the Chair of the Analog Signal Processing Technical Committee of the IEEE Circuits and Systems (CAS) Society, an Analog Signal Processing Track Cochair for the International Conference on Environmental and Computer Science (ICECS) 2004, a member of the Technical Program Committee for the 2004 International Workshop on Biomedical Circuits and Systems, a member of the International Program Committee for the International Association of Science and Technology for Development International Conference on Circuits, Signals, and Systems (IASTED CSS) 2005, and CSS 2006, a member of the Technical Program Committee for the Asia Pacific Conference on Circuits and Systems (APCCAS) 2006, a member of the Technical Program Committee for the IEEE Biomedical Circuits and Systems Conference (BioCAS 2006, BioCAS 2007, and BioCAS 2008), a Special-Session Co-Chair for ISCAS 2007, a member of the CAS Long-Term Strategy Committee. He is currently a member of the Board of Governors (BoG) of the Circuits and Systems Society (second term), a member of the Conference Division of the CAS BoG, a Deputy Editor-in-Chief of theIEEE TRANSACTIONS ON CIRCUITS AND SYSTEMS—I: REGULAR PAPERS, and a member of the International Program Committee of the 2009 International Conference on Biomedical Electronics and Devices, a Special Session Cochair for ISCAS 2009, a Special Session Cochair for ICECS 2009, and a member of the Technical Program Committee for ICUWB 2009. Recently, he was elected as the Technical Program Chair for the ISCAS 2010. He is currently the Editor-in-Chief of IEEE TRANSACTIONS ON CIRCUITS AND SYSTEMS—I: REGULAR PAPERS.

John R. Long (M'95) received the B.Sc. degree in electrical engineering from the University of Calgary, Calgary, AB, Canada, in 1984, and the M.Eng. and Ph.D. degrees in electronics from Carleton University, Ottawa, ON, Canada, in 1992 and 1996, respectively.

For ten years, he was at Bell-Northern Research, Ottawa (now Nortel Networks R&D), where he was involved in the design of application-specified integrated circuits (ASICs) for Gbit/s fiber-optic transmission systems,. From 1996 to 2001, he was an Assistant and then an Associate Professor at the University of Toronto, Canada. Since January 2002, he has been the Chair of the Electronics Research Laboratory, Delft University of Technology, Delft, The Netherlands. His current research interests include transceiver circuits for integrated wireless and high-speed wireline data communications systems.

Prof. Long is a former Associate Editor of the IEEE JOURNAL OF SOLID-STATE CIRCUITS, and is currently a Distinguished Lecturer with the Solid-State Circuits Society. He received the Natural Sciences and Engineering Research Council (NSERC) Doctoral Prize and Douglas R. Colton and Governor General's Medals for research excellence, and is a corecipient of the Best Paper Awards from the International Solid-State Circuits Conference (ISSCC) in 2000 and 2007, the RFIC and the European Wireless Symposia in 2006, and IEEE-BCTM in 2003. He was the General Chair and a Local Organizer for the 2006 IEEE Bipolar/BiCMOS Circuits and Technology Meeting (BCTM), held in Maastricht, NL. He chairs the RF circuits subcommittee for ISSCC 2010, and is a member of the technical program committees for the European Solid-State Circuits (ESSCIRC) and European Microwave IC (EuMIC) conferences.